Biophysical Reports

REPORT

The space between us: Modeling spatial heterogeneity in synthetic microbial consortia dynamics

Ryan Godin,[1,2,3,4] Bhargav R. Karamched,[5,6,7,*] and Shawn D. Ryan[3,4,*]

[1]Department of Chemical and Biological Engineering, Iowa State University, Ames, Iowa; [2]Department of Biology, Geology, and Environmental Sciences, Cleveland State University, Cleveland, Ohio; [3]Department of Mathematics and Statistics, Cleveland State University, Cleveland, Ohio; [4]Center for Applied Data Analysis and Modeling, Cleveland State University, Cleveland, Ohio; [5]Department of Mathematics, Florida State University, Tallahassee, Florida; [6]Institute of Molecular Biophysics, Florida State University, Tallahassee, Florida; and [7]Program in Neuroscience, Florida State University, Tallahassee, Florida

ABSTRACT A central endeavor in bioengineering concerns the construction of multistrain microbial consortia with desired properties. Typically, a gene network is partitioned between strains, and strains communicate via quorum sensing, allowing for complex behaviors. Yet a fundamental question of how emergent spatiotemporal patterning in multistrain microbial consortia affects consortial dynamics is not understood well. Here, we propose a computationally tractable and straightforward modeling framework that explicitly allows linking spatiotemporal patterning to consortial dynamics. We validate our model against previously published results and make predictions of how spatial heterogeneity impacts interstrain communication. By enabling the investigation of spatial patterns effects on microbial dynamics, our modeling framework informs experimentalists, helps advance the understanding of complex microbial systems, and supports the development of applications involving them.

SIGNIFICANCE Multistrain microbial consortia are able to accomplish tasks difficult to engineer in any one strain. Thus, substantial research in bioengineering has focused on the construction of multistrain microbial consortia with desired properties. Yet how emergent spatiotemporal patterning affects consortial dynamics is still poorly understood. A better understanding of this effect can aid the development and deployment of microbial consortia for various biotechnology applications. Toward this goal, we propose a computationally tractable and straightforward modeling framework that explicitly allows linking spatiotemporal patterning to consortial dynamics. Furthermore, our framework is flexible and generalizes to a wide range of applications.

INTRODUCTION

Since the discovery of quorum sensing in the early 1970s (1), understanding of microbial communication has grown tremendously. Multiple communication mechanisms such as acyl-homoserine lactones (AHLs) (2, 3) and autoinducing polypeptides (AIPs) (4, 5) have been uncovered, and their role in the formation of complex social behaviors such as biofilms and swarming motility have been deciphered (6–8). Recognizing that consortia of interacting microbial populations can perform more complicated behaviors than any one species individually, researchers have begun to leverage these systems for various biotechnology applications (9). For example, microbial consortia have been designed using natural or genetically engineered bacterial strains for use in biosensors (10), bioremediation (11, 12), and more efficient bioproduction (13–15). With this wide level of utility, the impact of microbial consortia on industry and human health are likely to grow as more efficient tools are developed for their design and application.

Substantial tools exist for controlling a particular consortium's behavior genetically using synthetic regulatory circuits (16–19), and tools for engineering a consortium's spatial organization have also begun to be developed (20). For example, Romano et al. recently developed a novel optogenic method for regulating gene expression that allowed them to re-create highly complex images using bacterial lawns (21). Similarly, Alnahhas et al. demonstrated that the number of subpopulation bands in an extended microfluidic device

Submitted August 12, 2022, and accepted for publication November 14, 2022.

*Correspondence: bkaramched@fsu.edu or s.d.ryan@csuohio.edu

Bhargav R. Karamched and Shawn D. Ryan contributed equally.

Editor: Jorg Enderlein.

https://doi.org/10.1016/j.bpr.2022.100085

can be regulated through the seeding of the trap. Other methods for regulating the spatial organization of consortia including adhesion, cell-communication, and motility are also being developed (20, 22–26). With previous studies demonstrating that the spatial organization of a consortium can significantly alter its dynamics (18, 27), these experimental methods are enabling an additional layer of control for engineering microbial consortia.

What is lacking from the research are sufficiently flexible modeling frameworks for investigating the impact of complex spatiotemporal structure on microbial consortium dynamics. These tools have the potential to streamline the rational engineering of spatial patterns to control consortium behavior. Previous approaches to modeling the spatiotemporal dynamics of microbial consortia have traditionally relied on well-mixed compartment models (16, 17) or agent-based frameworks (28–30). However, the well-mixed compartment models do not allow for the explicit incorporation of strain patterns, and agent-based modeling frameworks are computationally expensive for larger systems (31). To address this gap in the literature, we borrow from previous research focused on modeling diffusion in heterogeneous media (32–34) and develop a piecewise-defined reaction-diffusion equation framework for modeling spatiotemporal consortium dynamics. Here, we show that this modeling framework allows for the explicit incorporation of consortium spatial organization while remaining computationally tractable for larger systems. We then use this framework to investigate the impact of spatial heterogeneity on consortium dynamics and, using our results, demonstrate the rational design of consortium dynamics through spatial organization. Importantly, our framework provides an explicit link between interstrain communication and spatiotemporal patterning.

Modeling framework

For diffusion in heterogeneous media, variations in the composition of the medium results in corresponding discontinuities in its physical properties that need to be accounted for when modeling molecular transport. Researchers traditionally model this phenomenon using a reaction-diffusion equation (32–34):

$$\frac{\partial c}{\partial t} - \nabla\cdot\nabla(D(\mathbf{x})c(\mathbf{x},t)) = f(c,\mathbf{x},t),$$
$$t \geq 0,\ \mathbf{x} = (x,y,z) \in \Omega,$$

(Reaction-Diffusion Equation)

where $c = c(\mathbf{x},t)$ is the local concentration of the diffusing molecule, D is the diffusion coefficient, t is time, Ω is the domain, and $f(c,\mathbf{x},t)$ describes the production and degradation of c. To account for variations in transport properties in heterogeneous media, D is piecewise-defined according to the medium composition to have the appropriate value in the appropriate (user-controlled) location. Recognizing a natural correspondence between media heterogeneity and cell heterogeneity, we modify this modeling approach so that it can be used to study the spatiotemporal dynamics of microbial consortia. In our modified approach, the concentration of each signaling molecule in the consortium is modeled using a reaction-diffusion equation with components representing the local production and degradation described by a source term $f(c,\mathbf{x},t)$. We incorporate the spatial organization of the consortium strains into the resulting partial differential equation (PDE) model by structuring the source term for each signaling molecule on Ω as a piecewise function. This ensures that each signal is only generated in areas that contain a strain capable of producing it. Since each strain is uniquely defined by the signaling molecules that it produces, piecewise defining our system creates areas of production that mimic the spatial organization of the strains (see Fig. 1 *A*). This allows the resulting system to incorporate the influence of spatial organization on the dynamics of the microbial consortium and allows for the investigation of any desired organization.

Evaluation of framework and results

As a first application of this framework, we used it to model a recent experimental study of the spatiotemporal dynamics of a well-known microbial consortium (16). There, Kim et al. compared the dynamics of four microbial consortia in a spatially extended microfluidic trap consisting of different types of feedback networks. Each consortium consisted of an activator and repressor microbial strain in an alternating columnar spatial arrangement (diagrammed in Fig. 1 *A*). The two strains regulated each other's gene expression in a dual-feedback mechanism to produce an oscillating fluorescent pattern (17). Through experimentation and modeling, Kim et al. found that the addition of a positive feedback loop resulted in globally coordinated oscillations. This was in spite of the fact that the length of the trap was significantly larger than the diffusion correlation length of the signaling molecules, thereby preventing direct communication between strains located far apart from each other (16). However, their model omitted the organization of the stripe spatial patterns. Stripe thickness could affect the ability of the strains to couple their behavior through diffusion. Thus, the influence of strain spatial organization on consortium dynamics warrants investigation. For simplicity, we only model two of the

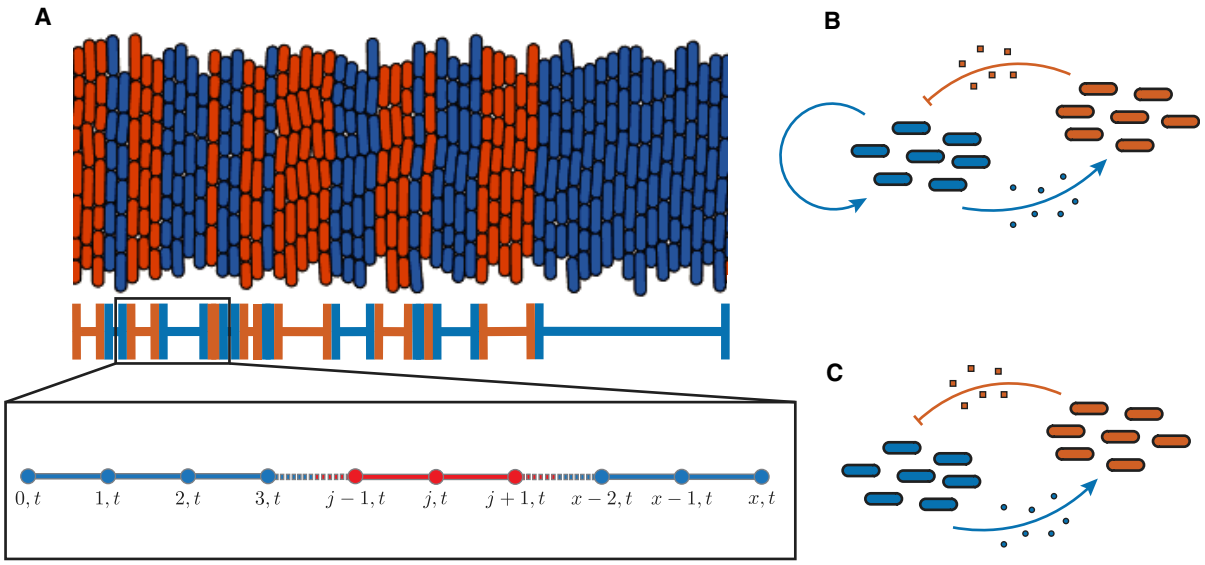

FIGURE 1 Consortial organization. (*A*) Micro and macro illustration of our spatial discretization that allows for the incorporation of columnar spatial patterns in the $\boldsymbol{P_2N_1}$ and $\boldsymbol{P_1N_1}$ consortia. For spatial points corresponding to activator segments (blue), the production terms for the repressor, η_{r_0} and η_{r_1}, are set to zero. The opposite holds in the repressor segments (orange) where the the production terms for the activator, η_{a_0} and η_{a_1}, are set to zero. Diagram of the $\boldsymbol{P_2N_1}$ (*B*) and $\boldsymbol{P_1N_1}$ (*C*) gene circuit topology.

consortia studied in Kim et al., P_2N_1 and P_1N_1 (diagrammed in Fig. 1 *B* and *C*), since they behave very similarly to the other two consortia. The P_2N_1 and P_1N_1 consortia also exhibited more robust columnar stripe patterns making them better suited to study in 1D.

Model derivation

To model the spatiotemporal dynamics of the P_2N_1 and P_1N_1 consortia using our framework, we constructed reaction-diffusion equations describing the dynamics of the consortium's extracellular signaling molecules. Like previous research into microbial consortia (35), we developed a simplified model of the dynamics since a thorough description of the underlying gene circuit interactions has been previously shown to require 16 delay-differential equations (DDEs) (17). To do so, we suppressed the dynamics of the fluorescent reporters and considered only the dynamics of the extracellular signaling molecules. This simplification is valid because the fluorescent reporters are produced in proportion to the local concentration of the lactone-based signaling molecules (17). We also ignored the role of intermediaries in producing these signaling molecules by modeling their production using Langmuir-functions, which take into account the overall activator-repressor network interactions. These functions mirror the form of previously developed equations for modeling production in consortia (16, 17) and are provided below, where a represents the local concentration of the activator N-butanoyl-L-homoserine lactone (C4-HSL, C4) and r represents the local concentration of the repressor N-(3-hydroxytetradecanoyl)-DL-homoserine lactone (3-OHC14-HSL, C14). We chose a similar strategy to model their enzymatic degradation by AHL-lactonase, AiiA, since it is produced in response to the local concentration of the repressor. We also borrowed from previous research by assuming linear degradation of the signaling lactones and a 7.5-min transcriptional delay, τ (16, 17).

With these interactions characterized, the source terms $f_a(\mathbf{x},t)$ and $f_r(\mathbf{x},t)$ are given by

$$f_a(\mathbf{x},t) = \underbrace{\frac{\eta_{a_0}+\eta_{a_1}\left(\frac{a_\tau}{K_a}\right)^{n_a}}{1+\left(\frac{a_\tau}{K_a}\right)^{n_a}+\left(\frac{r_\tau}{K_r}\right)^{n_r}}}_{\text{production}} - \underbrace{\frac{d_e a\left(\frac{r_\tau}{K_e}\right)^{n_e}}{1+\left(\frac{r_\tau}{K_e}\right)^{n_e}}}_{\text{AiiA degradation}} - \underbrace{\gamma a}_{\text{dilution}} \quad (1)$$

$$f_r(\mathbf{x},t) = \underbrace{\frac{\eta_{r_0}+\eta_{r_1}\left(\frac{a_\tau}{K_a}\right)^{n_a}}{1+\left(\frac{a_\tau}{K_a}\right)^{n_a}}}_{\text{production}} - \underbrace{\frac{d_e r\left(\frac{r_\tau}{K_e}\right)^{n_e}}{1+\left(\frac{r_\tau}{K_e}\right)^{n_e}}}_{\text{AiiA degradation}} - \underbrace{\gamma r}_{\text{dilution}}, \quad (2)$$

where $a_\tau \equiv a(\mathbf{x},t-\tau)$ and $r_\tau \equiv r(\mathbf{x},t-\tau)$. A complete description of all the parameters and their corresponding values can be found below in Table 1, and a description of how the parameters values were determined can be found in the Methods section of the Supporting

TABLE 1 Parameter Values and Descriptions

Parameter	Description	Value
η_{a_0}	Basal production rate of activator signaling molecule from promoter.	$985.56\ \text{nM}\ \text{min}^{-1}$
η_{a_1}	Maximal production rate of activator signaling molecule from promoter in response to activator signal.	$17,991.82/0\ \text{nM}\ \text{min}^{-1}$
η_{r_0}	Basal production rate of repressor signaling molecule from promoter.	$74.46\ \text{nM}\ \text{min}^{-1}$
η_{r_1}	Maximal production rate of repressor signaling molecule from promoter in response to activator signal.	$46,495.80\ \text{nM}\ \text{min}^{-1}$
K_a	EC_{50} of activator signaling molecule for production.	5937 nM
K_r	IC_{50} of repressor signaling molecule for repression.	10 nM
n_a	Langmuir coefficient of production for activator signaling molecule.	4
n_r	Langmuir coefficient of repression for repressor signaling molecule.	2
D	Diffusion coefficient signaling molecules.	$4080\ \mu\text{m}^2\ \text{min}^{-1}$
d_e	Maximal rate of internal enzymatic degradation of signaling molecules.	$2257\ \text{min}^{-1}$
K_e	EC_{50} of repressor signaling molecule for enzymatic degradation.	1000 nM
n_e	Langmuir coefficient of internal enzymatic degradation for repressor signaling molecule.	4
γ	Inherent rate of degradation of signaling molecules caused by dilution from both media flow and cell growth.	$0.128\ \text{min}^{-1}$
τ	Time delay for transcription and translation.	7.5 min

material. To differentiate between the P_2N_1 and P_1N_1 consortia, η_{a_1} is set to zero for the P_1N_1 consortium to account for the absence of the auto-activation, and the $\left(\frac{a_\tau}{K_a}\right)^{n_a}$ in the denominator of the production term is removed. We thus arrived at the following two-equation system, partial delay-differential equation model of the P_2N_1 and P_1N_1 consortium spatiotemporal dynamics:

$$\begin{cases} \dfrac{\partial a}{\partial t} - D\nabla^2 a = f_a(\mathbf{x},t) \\ \dfrac{\partial r}{\partial t} - D\nabla^2 r = f_r(\mathbf{x},t) \end{cases} \tag{3}$$

The strain spatial organizations are included in this model in a user-defined fashion through the piecewise definition of $f_a(\mathbf{x},t)$ and $f_r(\mathbf{x},t)$. Specifically, we set the production rate terms in $f_a(\mathbf{x},t)$ and $f_r(\mathbf{x},t)$ to be zero in areas that did not include an activator or repressor strain, respectively.

Model validation

To validate our simplified model of the P_2N_1 and P_1N_1 consortia, we investigated its ability to accurately capture the spatiotemporal dynamics recently observed in Kim et al. The main result of this paper was that strains containing a second positive feedback loop synchronized their dynamics across a spatially extended microfluidic trap. Thus, we validated our model by testing whether it could reproduce this key behavior. For this test, we simulated the P_2N_1 and P_1N_1 consortia in one dimension. A 1D model was chosen since diffusion and variations in strain composition in the vertical direction are assumed to be negligible in the spatially extended trap (16). We therefore modeled the $L = 2$ mm long trap (e.g., device size in Kim et al. (16)) using the 1D spatial domain, $\Omega \equiv [0, L]$. The consortia were implemented by dividing the spatial domain into 100 stripes of equal width alternating between activator and repressor strains. The consortium was then divided into two equally spaced halves oscillating with an initial phase difference of $|\Delta\varphi_0| = 25\%$ of the oscillation period, φ. We chose this value because it resulted in synchrony for P_2N_1 and asynchrony for P_1N_1 in Kim et al. Both the P_2N_1 and P_1N_1 consortia were then analyzed for whether synchronization between the two halves occurred. To determine the presence of synchronization, we calculated the phase difference of the activator concentration oscillations for the middle spatial points of the left and right subpopulations, Δt_φ (detailed explanation provided in the Methods section of the Supporting material). A percent phase difference, $|\Delta\varphi|$ was then calculated as follows:

$$|\Delta\varphi| = \frac{\Delta t_\varphi}{\varphi} * 100 \tag{4}$$

We assumed a phase difference of $|\Delta\varphi| < 2.5\%$ between the two halves corresponded to synchronization across the trap. Since φ depends on the basal production rate, η_{a0}, we chose to measure the phase difference after the 10th oscillation instead of after a specified period of time had passed.

The presence of the autoinducing positive feedback loop in the P_2N_1 consortium was cited in Kim et al. as the reason P_2N_1 oscillations became coordinated, whereas P_1N_1 oscillations did not. Thus, we originally only varied the value of η_{a_1} between our P_2N_1 and P_1N_1 simulations, setting it to zero in the P_1N_1 simulation to account for an absence of the feedback loop.

We failed to see any significant difference in coordination between the P_2N_1 and P_1N_1 consortia (Fig. 2 *C*). With this finding, it was clear that the difference in the activator basal production rate between the P_2N_1 and P_1N_1 consortia needed to be incorporated into our model. In Chen et al., it was reported that the activator basal production rate in the P_1N_1 consortium is approximately nine times greater than in the P_2N_1 consortium, and this difference was even included in the model used in Kim et al. Thus, to investigate the role changing this basal production rate had on P_1N_1 behavior, we re-ran the P_1N_1 synchronization tests for different values of η_{a_0}. Specifically, we scaled η_{a_0} by a basal multiplier, b_m, that varied from 0.1 to 10. The results of these tests are provided in Fig. 2 *C* and show that the coordination of oscillations is strongly influenced by the value of the activator basal production rate, η_{a_0}. Kymographs illustrating the level of coordination in the P_2N_1 and P_1N_1 consortia are provided in Fig. 2 *A* and *B*, respectively.

Investigating the role of spatial heterogeneity

Having validated our model against the experimentally observed difference between the P_2N_1 and P_1N_1 consortia, provided the difference in activator basal production rates is incorporated, we proceeded to test our model's ability to capture the influence of spatial heterogeneity on consortium dynamics. This is the primary focus of this work and will provide new insight into heterogeneous systems. First, we investigated the impact changing stripe width had on the coordination of oscillations in the P_2N_1 consortium. This was done by repeating the aforementioned synchronization

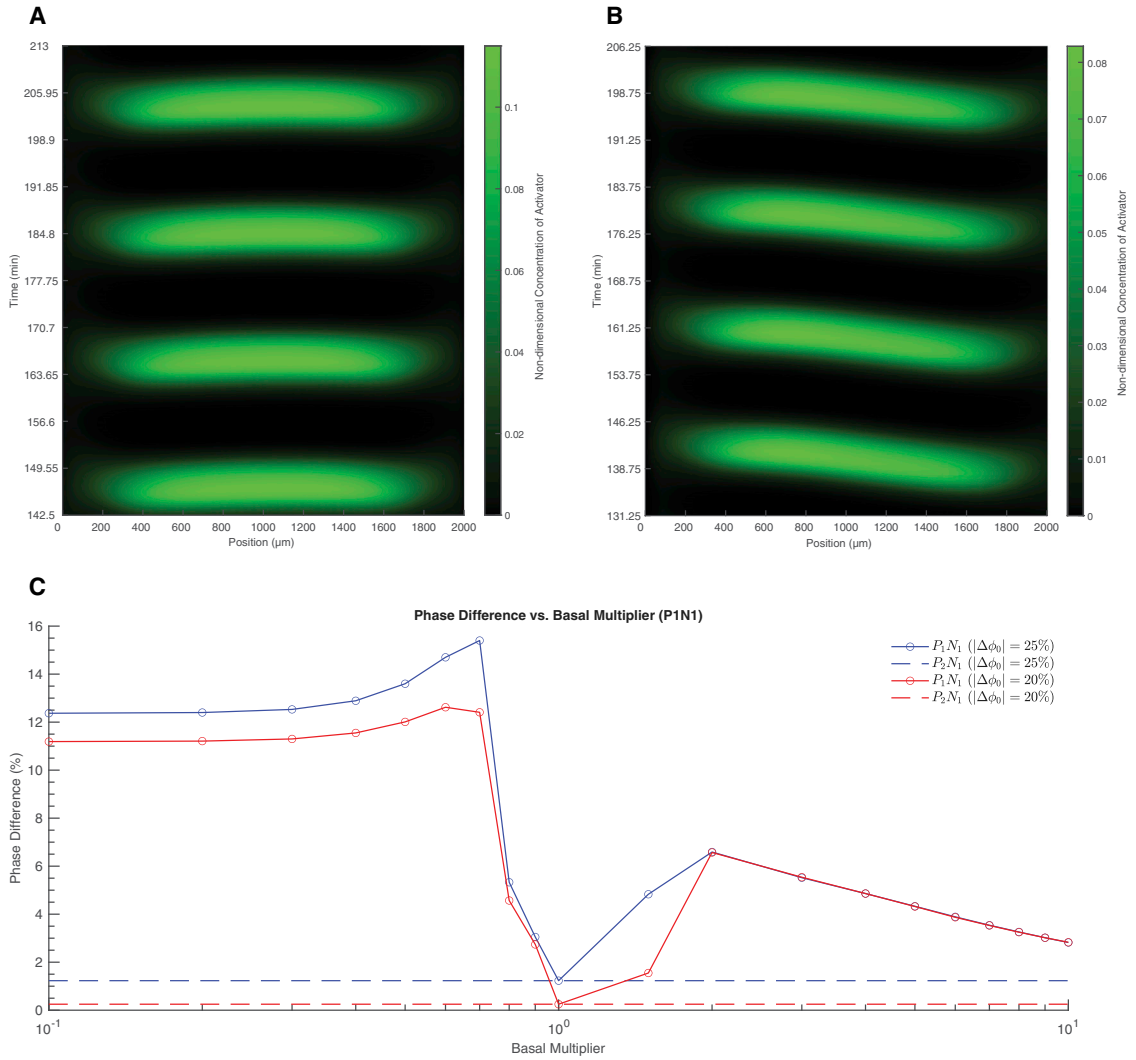

FIGURE 2 Basal production's influence on synchrony. Results of our synchronization simulations including kymograph of activator concentration during the 8th to 11th oscillations of the $\boldsymbol{P_2N_1}$ (*A*) and $\boldsymbol{P_1N_1}$ (*B*) consortia (basal multiplier of 0.7). (*C*) Graph showing the relationship between phase difference and the value of the basal multiplier for the $\boldsymbol{P_1N_1}$ consortium at two different initial phase differences, $|\Delta\varphi_{\mathbf{0}}| = \mathbf{25}\%$ and $\mathbf{20}\%$.

test for the P_2N_1 consortium with stripe widths varying from 10 to 200 μm. The results of these simulations are provided in Fig. 3 *B* and show that coordination breaks down as stripe width increases. In fact, we observe a significant breakdown in synchrony for stripe widths larger than 90 μm. This shows quantitative agreement with previous experimental studies of the same consortia in Gupta et al. There, they found that separation distances larger than 100 μm between activator and repressor populations led to a loss of oscillatory behavior. This demonstrates that our modeling framework results are consistent with experimental results from different studies (16, 18).

Interestingly, a stripe width of 70 μm is optimal for synchronization. We intuit this result as follows. For stripe widths larger than 70 μm, the diffusion correlation length of the quorum sensing molecules is not great enough to allow for interstrain communication. That is, the coupling is too weak. On the other hand, for stripe widths less than 70 μm, chemical signals can diffuse across several stripes, flooding the trap with chemical signal. When active, the activator promoters are maximally productive, leading to an effective basal production rate that corresponds to the right-hand side of Fig. 2 *C*. In effect, the spatial heterogeneity provides an engineering methodology to control the effective basal production of the strains.

With this result in mind, we hypothesized that the coordination of the consortium could be controlled by only varying its spatial organization. To test this hypothesis, we simulated two P_2N_1 consortia side by side in a 4-mm-long trap. Both consortia contained alternating activator and repressor stripes whose widths increased linearly. However, the first consortium contained small-width stripes (0.56–47.06 μm), and the second consortium contained large-width stripes (19.05–266.67 μm). The results of this test are provided in a kymograph showing the concentration of the activator across the consortium and time. As anticipated by the results provided in Fig. 3 *B*, the left half of the consortium oscillated in a coordinated manner, and the right half of the consortium, containing larger stripes, had its oscillations become decoupled.

DISCUSSION

We developed a new modeling framework to investigate the impact of spatial heterogeneity on consortial dynamics. We verified our framework results against the modeling and experimental results found in Kim et al. (16). We also observed quantitative agreement between our stripe width investigation study and experimental findings from Gupta et al. (18). Although our model is much simpler than what is used by Kim et al. and coarse-grains over many subcellular processes, the qualitative behaviors of the two models coincide. Our model gains tractability at the expense of some fidelity to reality. But it is exactly in these scenarios that mathematical modeling can provide unexpected qualitative predictions regarding the biological system.

The results demonstrate that our new modeling framework is able to effectively incorporate the effect of spatial organization on microbial consortium dynamics. By allowing for the explicit incorporation of stripe patterns, our work complements and extends previous research into modeling spatiotemporal dynamics of microbial consortia (16, 18, 22, 28–30, 36, 37). For example, Kim et al. modeled spatiotemporal dynamics using well-mixed compartments containing both activator and repressor strains. However, this approach prevents the incorporation of well-defined

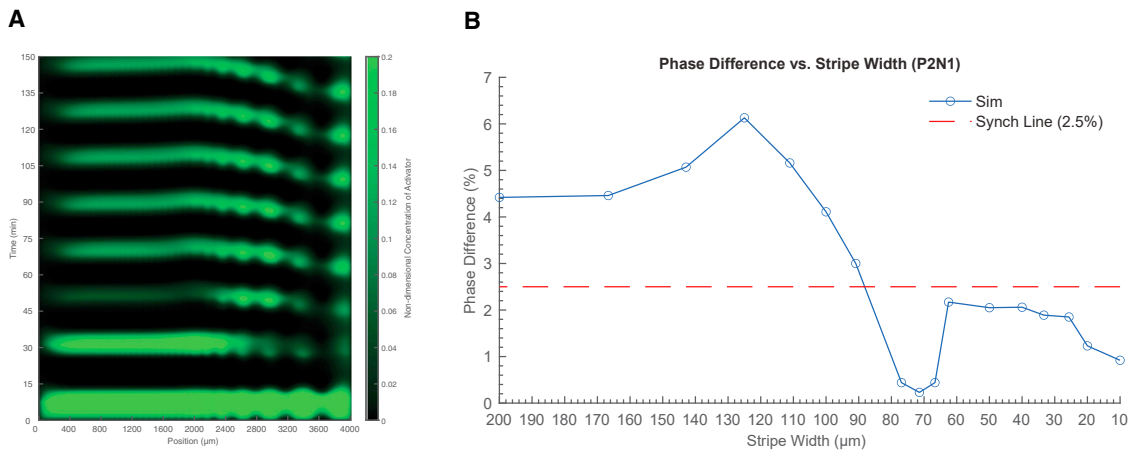

FIGURE 3 Spatial organization's influence on synchrony. (*A*) Kymograph of activator concentration in the $\boldsymbol{P_2N_1}$ consortium consisting of heterogeneous stripes. The left side of the consortium consists of small-width stripes (0.56–47.06 μm), and the right side of the consortium consists of large-width stripes (19.05–266.67 μm). (*B*) Graph showing the relationship between phase difference and stripe width for the $\boldsymbol{P_2N_1}$ consortium.

spatial patterns into the consortia, which, in turn, limits any investigation into their effect on consortium dynamics. Our piecewise-defined diffusion equation framework allowed us to investigate this impact in the present study. Our modeling framework is thus more faithful to the robust single-strain stripes observed in Alnahhas et al. Compartment models force all cells in a given compartment to experience the same level of chemical signal. Our piecewise framework allows for spatial variations *within and between* single-strain stripes.

As expected, we found that small-width stripes allowed for more coordination of consortium dynamics due to better communication between stripes over shorter distances (18, 27). Interestingly, our heterogeneous stripe test demonstrates consortium behavior can be controlled through the consortium's spatial organization alone. Combined with a rise in experimental methods for controlling spatial organizations in consortia (20, 23, 24, 38), this opens an interesting avenue for regulating consortium dynamics in the future (36).

An unexpected finding from our work was the strong influence of the basal multiplier on consortium coordination. From the results of Kim et al., it was expected that the presence or absence of the positive feedback loop would be sufficient to control coordination. Our simulation results indicate that the basal production rate had a stronger impact. Since the results of the basal multiplier test mirror that of the stripe width investigation (see Figs. 2 *C* and 3 *B*), we hypothesize that the observed behavior was due to variations in communication strength at various multiplier values. For lower values, the production rate of signaling molecule is lower, which results in weaker signaling between stripes. The opposite holds for higher production rates. The fact that Kim et al. included differences in basal production rates into their model may have obfuscated the actual impact of the positive feedback loop. However, since our model substantially simplifies the underlying gene circuits in exchange for computational efficiency and understandability, the basal multiplier results could be an artifact of this simplification.

Separate from this simplified model is the underlying framework of using piecewise-defined reaction-diffusion equations to incorporate spatial patterns into studies on consortium dynamics. Our ability to study various spatial patterns using this framework demonstrates its usefulness for modeling the spatiotemporal dynamics of microbial consortia. One strength of this framework is its flexibility. By varying the spatial points where the production terms are nonzero, a researcher can precisely control the spatial organization they are studying, including heterogeneous arrangements. Besides flexibility, another benefit of our model is its computational tractability. One strategy that previous studies have used to explicitly incorporate consortium spatial patterns is agent-based modeling (28–30). Although the fine-grained nature of these frameworks provides the greatest level of control when investigating the impact of spatial patterns, the complexity of these systems makes the study of larger consortia computationally infeasible (29, 31). Our continuum-based framework complements these studies and fills a gap in the literature by allowing for incorporation of spatial organizations into studies on the dynamics of large, spatially extended consortia.

Although we did not investigate other geometries or consortia in this study, we are confident the flexibility and computational tractability of our modeling framework will enable the study of more complicated systems. For example, our model could be used to investigate the effects of square size on consortium dynamics for the checkerboard pattern recently developed by Perkins et al. Besides allowing for a better understanding of these systems, our heterogeneous stripe results show that our modeling framework could potentially be used to engineer consortium behavior by finding spatial organizations that modulate the communication between consortium subpopulations in a desired fashion. Specifically, this can be done by making the distance between subpopulations either smaller or larger to modify the signaling strength between the subpopulations. We used this principle here to design a consortium that oscillated synchronously on the half that contained small stripes and asynchronously on the half that contained large stripes. Combined with a growing number of experimental approaches for designing consortia with specific spatial arrangements, including optogenic, seeding, and other approaches (20, 22–24), modulating consortium dynamics through spatial organization is becoming more practical. Since the underlying numerical scheme used to solve our reaction-diffusion equation model has routinely been applied in higher dimensions (39–42), our framework is well suited to interrogate the effects of the more complex spatial organizations implemented by these experimental methods (23, 43–45). Through enabling these investigations into the impact of spatial organization on microbial consortium dynamics, we hope that our modeling framework helps advance the understanding of these systems and supports the development of new applications involving them.

CODE AVAILABILITY

The input MATLAB scripts used in our simulations and representative examples from this work are available for download from GitHub: https://github.com/sdryan/StripeHeterogeneity.

SUPPORTING MATERIAL

Supporting Material can be found online at https://doi.org/10.1016/j.bpr.2022.100085.

AUTHOR CONTRIBUTIONS

R.G., B.R.K., and S.D.R. conceived the problem and built the mathematical model. R.G. and S.D.R. designed the numerical approach and conducted the numerical simulations. B.RK. provided background in modeling microbial consortia. R.G. prepared the manuscript after careful discussion with B.R.K. and S.D.R. R.G., B.R.K., and S.D.R. edited the paper.

ACKNOWLEDGMENTS

R.G., S.D.R., and B.R.K. would like to thank Mehdi Sadeghpour for insightful discussions. R.G. and S.D.R. would like to thank the CSU Research Center for Applied Data Analysis and Modeling (ADAM) for support throughout the project. B.R.K. would like to thank the FSU Systems and Computational Understanding of Biophysical Actions (SCUBA) group for support. B.R.K. would like to thank his wife, Hajra Habib, for her unending support. R.G. began the project at CSU and finished at ISU.

DECLARATION OF INTERESTS

The authors declare no competing interests.

REFERENCES

1. Nealson, K. H., T. Platt, and J. W. Hastings. 1970. Cellular control of the synthesis and activity of the bacterial luminescent system. *J. Bacteriol.* 104:313–322.
2. Parsek, M. R., D. L. Val, …, E. P. Greenberg. 1999. Acyl homoserine-lactone quorum-sensing signal generation. *Proc. Natl. Acad. Sci. USA.* 96:4360–4365.
3. Miano, A., M. J. Liao, and J. Hasty. 2020. Inducible cell-to-cell signaling for tunable dynamics in microbial communities. *Nat. Commun.* 11:1193–1198.
4. Vasquez, J. K., and H. E. Blackwell. 2019. Simplified autoinducing peptide mimetics with single-nanomolar activity against the Staphylococcus aureus AgrC quorum sensing receptor. *ACS Infect. Dis.* 5:484–492.
5. Ji, G., R. C. Beavis, and R. P. Novick. 1995. Cell density control of staphylococcal virulence mediated by an octapeptide pheromone. *Proc. Natl. Acad. Sci. USA.* 92:12055–12059.
6. Hammer, B. K., and B. L. Bassler. 2003. Quorum sensing controls biofilm formation in Vibrio cholerae. *Mol. Microbiol.* 50:101–104.
7. An, J. H., E. Goo, …, I. Hwang. 2014. Bacterial quorum sensing and metabolic slowing in a cooperative population. *Proc. Natl. Acad. Sci. USA.* 111:14912–14917.
8. Shrout, J. D., D. L. Chopp, …, M. R. Parsek. 2006. The impact of quorum sensing and swarming motility on Pseudomonas aeruginosa biofilm formation is nutritionally conditional. *Mol. Microbiol.* 62:1264–1277.
9. Cavaliere, M., S. Feng, …, J. I. Jiménez. 2017. Cooperation in microbial communities and their biotechnological applications. *Environ. Microbiol.* 19:2949–2963.
10. Khatun, M. A., M. A. Hoque, …, Y. Feng. 2018. Bacterial consortium-based sensing system for detecting organophosphorus pesticides. *Anal. Chem.* 90:10577–10584.
11. Feng, S., L. Gong, …, H. Yang. 2021. Bioaugmentation potential evaluation of a bacterial consortium composed of isolated Pseudomonas and Rhodococcus for degrading benzene, toluene and styrene in sludge and sewage. *Bioresour. Technol.* 320:124329.
12. Nayak, J. K., R. Gautam, and U. K. Ghosh. 2022. Bioremediation potential of bacterial consortium on different wastewaters for electricity and biomass feedstock generation. *Biomass Convers. Biorefin.* 1–14.
13. Wu, S., J. Qiao, …, C. Liu. 2022. Potential of orthogonal and cross-talk quorum sensing for dynamic regulation in cocultivation. *Chem. Eng. J.* 445:136720.
14. Joshi, C., S. Sharma, …, S. K. Masakapalli. 2020. Efficient system wide metabolic pathway comparisons in multiple microbes using genome to KEGG orthology (G2KO) pipeline tool. *Interdiscip. Sci.* 12:311–322.
15. Schlembach, I., H. Hosseinpour Tehrani, …, M. A. Rosenbaum. 2020. Consolidated bioprocessing of cellulose to itaconic acid by a co-culture of Trichoderma reesei and Ustilago maydis. *Biotechnol. Biofuels.* 13:207–218.
16. Kim, J. K., Y. Chen, …, M. R. Bennett. 2019. Long-range temporal coordination of gene expression in synthetic microbial consortia. *Nat. Chem. Biol.* 15:1102–1109.
17. Chen, Y., J. K. Kim, …, M. R. Bennett. 2015. Emergent genetic oscillations in a synthetic microbial consortium. *Science.* 349:986–989.
18. Gupta, S., T. D. Ross, …, O. S. Venturelli. 2020. Investigating the dynamics of microbial consortia in spatially structured environments. *Nat. Commun.* 11:2418.
19. Liao, M. J., M. O. Din, …, J. Hasty. 2019. Rock-paper-scissors: Engineered population dynamics increase genetic stability. *Science.* 365:1045–1049.
20. Barbier, I., H. Kusumawardhani, and Y. Schaerli. 2022. Engineering synthetic spatial patterns in microbial populations and communities. *Curr. Opin. Microbiol.* 67:102149.
21. Romano, E., A. Baumschlager, …, B. Di Ventura. 2021. Engineering AraC to make it responsive to light instead of arabinose. *Nat. Chem. Biol.* 17:817–827.
22. Alnahhas, R. N., J. J. Winkle, …, M. R. Bennett. 2019. Spatiotemporal dynamics of synthetic microbial consortia in microfluidic devices. *ACS Synth. Biol.* 8:2051–2058.
23. Perkins, M. L., D. Benzinger, …, M. Khammash. 2020. Cell-in-the-loop pattern formation with optogenetically emulated cell-to-cell signaling. *Nat. Commun.* 11:1355.
24. Barbier, I., R. Perez-Carrasco, and Y. Schaerli. 2020. Controlling spatiotemporal pattern formation in a concentration gradient with a synthetic toggle switch. *Mol. Syst. Biol.* 16:e9361.
25. Ryan, S. D., G. Ariel, and A. Be'er. 2016. Anomalous fluctuations in the orientation and velocity of swarming bacteria. *Biophys. J.* 111:247–255.
26. Ryan, S. D. 2019. Role of hydrodynamic interactions in chemotaxis of bacterial populations. *Phys. Biol.* 17:016003.
27. van Tatenhove-Pel, R. J., T. Rijavec, …, H. Bachmann. 2021. Microbial competition reduces metabolic interaction distances to the low μm-range. *ISME J.* 15:688–701.
28. Fiore, D., D. Salzano, …, M. di Bernardo. 2021. Multicellular feedback control of a genetic toggle-switch in microbial consortia. *IEEE Control Syst. Lett.* 5:151–156.
29. Winkle, J. J., B. R. Karamched, …, K. Josić. 2021. Emergent spatiotemporal population dynamics with cell-length control of synthetic microbial consortia. *PLoS Comput. Biol.* 17:e1009381.
30. Fiore, G., A. Matyjaszkiewicz, …, M. Di Bernardo. 2017. In-silico analysis and implementation of a multicellular feedback control strategy in a synthetic bacterial consortium. *ACS Synth. Biol.* 6:507–517.
31. Wilmoth, J. L., P. W. Doak, …, M. Fuentes-Cabrera. 2018. A microfluidics and agent-based modeling framework for investigating

spatial organization in bacterial colonies: the case of Pseudomonas aeruginosa and H1-Type VI secretion interactions. *Front. Microbiol.* 9:33.

32. Prager, S. 1960. Diffusion in inhomogeneous media. *J. Chem. Phys.* 33:122–127.

33. Kalnin, J., E. Kotomin, and J. Maier. 2002. Calculations of the effective diffusion coefficient for inhomogeneous media. *J. Phys. Chem. Solid.* 63:449–456.

34. Van Kampen, N. 1988. Diffusion in inhomogeneous media. *J. Phys. Chem. Solid.* 49:673–677.

35. Sadeghpour, M., A. Veliz-Cuba, …, M. R. Bennett. 2017. Bistability and oscillations in co-repressive synthetic microbial consortia. *Quant. Biol.* 5:55–66.

36. Wu, F., Y. Ha, …, L. You. 2022. Modulation of microbial community dynamics by spatial partitioning. *Nat. Chem. Biol.* 18: 394–402.

37. Liao, M. J., A. Miano, …, J. Hasty. 2020. Survival of the weakest in non-transitive asymmetric interactions among strains of e. coli. *Nat. Commun.* 11:6055.

38. Alnahhas, R. N., M. Sadeghpour, …, M. R. Bennett. 2020. Majority sensing in synthetic microbial consortia. *Nat. Commun.* 11:3659.

39. Rouf, H. K., F. Costen, and S. G. Garcia. 2009. 3D Crank-Nicolson finite difference time domain method for dispersive media. *Electron. Lett.* 45:961.

40. Sadrpour, S.-M., V. Nayyeri, and M. Soleimani. 2016. A new 2D unconditionally stable finite-difference time-domain algorithm based on the Crank-Nicolson scheme. . 2016 IEEE International Conference on Computational Electromagnetics (ICCEM). IEEE, pp. 55–57.

41. Singh, M. K., S. Rajput, and R. K. Singh. 2021. Study of 2D contaminant transport with depth varying input source in a groundwater reservoir. *Water Supply.* 21:1464–1480.

42. Yang, C., and T. Sun. 2022. Crank–Nicolson finite difference schemes for parabolic optimal Dirichlet boundary control problems. *Math. Methods Appl. Sci.* 45:7346–7363.

43. Curatolo, A. I., N. Zhou, …, J. Huang. 2020. Cooperative pattern formation in multi-component bacterial systems through reciprocal motility regulation. *Nat. Phys.* 16:1152–1157.

44. Duran-Nebreda, S., J. Pla, …, R. Solé. 2021. Synthetic lateral inhibition in periodic pattern forming microbial colonies. *ACS Synth. Biol.* 10:277–285.

45. Glass, D. S., and I. H. Riedel-Kruse. 2018. A synthetic bacterial cell-cell adhesion toolbox for programming multicellular morphologies and patterns. *Cell.* 174:649–658.e16.

Biophysical Reports, Volume *2*

Supplemental information

The space between us: Modeling spatial heterogeneity in synthetic microbial consortia dynamics

Ryan Godin, Bhargav R. Karamched, and Shawn D. Ryan

1. Methods

Determination of Parameter Values

In our model, there were 14 parameter values that needed to be determined: η_{a_0}, η_{a_1}, η_{r_0}, η_{r_1}, K_a, K_r, n_a, n_r, D, d_e, K_e, n_e, γ, τ. These parameter values and their description are provided below in Table 1. The parameters K_a, n_a, n_r, d_e, n_e, and τ were taken directly from Kim et al.. Specifically, they were assigned the value of the biological parameter corresponding to their function in the model: K_a was assigned the EC50 value for $P_{\text{rhl/lac-s}}$ activation by C4, n_a was assigned the Langmuir-coefficient value for C4 activation of $P_{\text{rhl/lac-s}}$, n_a was assigned the Langmuir-coefficient value for LacI repression of $P_{\text{rhl/lac-s}}$, d_e was assigned the value of the catalytic constant for C4 and C14 degradation by AiiA, n_e was assigned the Langmuir-coefficient value for P_{cin^*} activation by C14, and τ was assigned the value of the time delay for transcription and translation. The values for K_e and K_r were chosen to give good qualitative agreement with the experimental results, and the remaining parameter values were calculated from parameters reported in Kim et al. These calculations are provided below.

Table S1: Parameter Values, Descriptions, and Source

Parameter	Description	Value	Source
η_{a_0}	Basal production rate of activator signaling molecule from promoter.	985.56 nM min^{-1}	Calculated.
η_{a_1}	Maximal production rate of activator signaling molecule from promoter in response to activator signal.	17991.82/0 nM min^{-1}	Calculated
η_{r_0}	Basal production rate of repressor signaling molecule from promoter.	74.46 nM min^{-1}	Calculated
η_{r_1}	Maximal production rate of repressor signaling molecule from promoter in response to activator signal.	46495.80 nM min^{-1}	Calculated
K_a	EC50 of activator signaling molecule for production.	5937 nM	Kim et al.
K_r	IC50 of repressor signaling molecule for repression.	10 nM	
n_a	Hill coefficient of production for activator signaling molecule.	4	Kim et al.
n_r	Hill coefficient of repression for repressor signaling molecule.	2	Kim et al.
D	Diffusion coefficient signaling molecules.	4080 μm^2 min^{-1}	Calculated
d_e	Maximal rate of internal enzymatic degradation of signaling molecules.	2257 min^{-1}	Kim et al.
K_e	EC50 of repressor signaling molecule for enzymatic degradation.	1000 nM	
n_e	Hill coefficient of internal enzymatic degradation for repressor signaling molecule.	4	Kim et al.
γ	Inherent rate of degradation of signaling molecules caused by dilution from both media flow and cell growth.	0.128 min^{-1}	Calculated
τ	Time delay for transcription and translation.	7.5 min	Kim et al.

For diffusion, we made the simplifying assumption that that diffusion was the same for both

extracellular signaling molecules C4 and C14. Thus, we took the diffusion as the average of the reported diffusion values from Kim et al., D_H for the activator (C4) and D_I for the repressor (C14):

$$D = \frac{D_H + D_I}{2} \tag{1}$$

$$= \frac{4800\ \mu\text{m}^2\ \text{min}^{-1} + 3360\ \mu\text{m}^2\ \text{min}^{-1}}{2} \tag{2}$$

$$D = 4080\ \mu\text{m}^2\ \text{min}^{-1} \tag{3}$$

The parameter value for non-enzymatic degradation, γ, was calculated by summing the contributions of dilution from cell-growth, d, and media flow, μ_e:

$$\gamma = d + \mu_e \tag{4}$$

$$= \ln(2)/25\ \text{min}^{-1} + 0.1\ \text{min}^{-1} \tag{5}$$

$$\gamma = 0.128\ \text{min}^{-1} \tag{6}$$

The remaining parameters were the production rates for the extracellular signaling lactones: η_{a_0}, η_{a_1}, η_{r_0}, and η_{r_1}. These lactones upregulated or downregulated $P_{\text{rhl/lac-s}}$ which in turn produced the enzymes RhlI and CinI which are synthases that catalyze the production of C4 and C14, respectively. Thus, to estimate production rates for C4 and C14 from the reported production rates for RhlI and CinI in Kim et al., we made the simplifying assumption that each enzyme lasts 1 min on average before being degraded by ClpXP. With production rates for RhlI and CinI of 16 min^{-1} and 2 min^{-1} this implies that each RhlI produces 16 C4 on average and each CinI produces 2 C14 on average. Using this assumption, we can then calculate the production rates for C4 and C14 as follows. Note that in the following calculations, S_R and S_C were indeterminate scalings for the parameters that were estimated in Kim et al.. Additionally, η_{R_x} and η_{C_x} stand for the production rates of RhlI and CinI from the promoters $P_{\text{rhl/lac-s}}$ and $P_{\text{rhl/lac-w}}$, respectively.

$$\eta_{a_0} = 16 \cdot \eta_{R_0} \tag{7}$$

$$= 16 \cdot 20.13 \cdot S_R\ \text{nM}\ \text{min}^{-1} \tag{8}$$

$$= 16 \cdot 20.13 \cdot 3.06\ \text{nM}\ \text{min}^{-1} \tag{9}$$

$$\eta_{a_0} = 985.56\ \text{nM}\ \text{min}^{-1} \tag{10}$$

$$\eta_{a_1} = 16 \cdot \eta_{R_1} \tag{11}$$
$$= 16 \cdot 367.48 \cdot S_R \text{ nM min}^{-1} \tag{12}$$
$$= 16 \cdot 367.48 \cdot 3.06 \text{ nM min}^{-1} \tag{13}$$
$$\eta_{a_1} = 17991.82 \text{ nM min}^{-1} \tag{14}$$

$$\eta_{r_0} = 2 \cdot \eta_{C_0} \tag{15}$$
$$= 2 \cdot 1 \cdot S_C \text{ nM min}^{-1} \tag{16}$$
$$= 2 \cdot 1 \cdot 37.23 \text{ nM min}^{-1} \tag{17}$$
$$\eta_{r_0} = 74.46 \text{ nM min}^{-1} \tag{18}$$

$$\eta_{r_1} = 2 \cdot \eta_{C_1} \tag{19}$$
$$= 2 \cdot 624.44 \cdot S_C \text{ nM min}^{-1} \tag{20}$$
$$= 2 \cdot 624.44 \cdot 37.23 \text{ nM min}^{-1} \tag{21}$$
$$\eta_{r_1} = 46495.80 \text{ nM min}^{-1} \tag{22}$$

Non-Dimensionalization

Our model was non-dimensionalized as follows. The activator and repressor concentrations were scaled by K_a, time was scaled by τ, and space was scaled by $\sqrt{D \cdot \tau}$. After introducing these scalings, the following system with non-dimensionalized parameters was obtained:

$$\begin{cases} \dfrac{\partial a}{\partial t} &= \dfrac{\eta_{as_0} + \eta_{as_1} a_\tau^{n_a}}{1 + a_\tau^{n_a} + \left(\frac{r_\tau}{K_{rs}}\right)^{n_r}} + D_s \dfrac{\partial^2 a}{\partial^2 x} - \dfrac{d_{es} a \left(\frac{r_\tau}{K_{es}}\right)^{n_e}}{1 + \left(\frac{r_\tau}{K_{es}}\right)^{n_e}} - \gamma_s a \\ \dfrac{\partial r}{\partial t} &= \dfrac{\eta_{rs_0} + \eta_{rs_1} a_\tau^{n_a}}{1 + a_\tau^{n_a}} + D_s \dfrac{\partial^2 r}{\partial^2 x} - \dfrac{d_{es} r \left(\frac{r_\tau}{K_{es}}\right)^{n_e}}{1 + \left(\frac{r_\tau}{K_{es}}\right)^{n_e}} - \gamma_s r \end{cases} \tag{23}$$

The parameters in the above system are defined as follows:

$$\eta_{as_0} = \frac{\eta_{a_0} \cdot \tau}{K_a} \tag{24}$$

$$\eta_{as_1} = \frac{\eta_{a_1} \cdot \tau}{K_a} \tag{25}$$

$$\eta_{rs_0} = \frac{\eta_{r_0} \cdot \tau}{K_a} \tag{26}$$

$$\eta_{rs_1} = \frac{\eta_{r_1} \cdot \tau}{K_a} \tag{27}$$

$$K_{rs} = \frac{K_r}{K_a} \tag{28}$$

$$D_s = 1 \tag{29}$$

$$d_{es} = d_e \cdot \tau \tag{30}$$

$$K_{es} = \frac{K_e}{K_a} \tag{31}$$

$$\gamma_s = \gamma \cdot \tau \tag{32}$$

Numerical Scheme and Synchronization Test Procedures

All simulations were performed in MATLAB 2020a using custom scripts. To carry out the synchronization test for the P_2N_1 and P_1N_1 consortia, the non-dimensionalized model, Equation 23, was implemented numerically using the Crank-Nicholson scheme in one spatial dimension. We chose to discretize space by constructing our spatial mesh out of 5,000 points with a non-dimensional spatial step of $\Delta x = \frac{2000\ \mu\text{m}}{\sqrt{D \cdot \tau}(5000)}$ and a time step of $\Delta t = 0.0001$. Here D is the signal diffusion strength and τ is the delay time. The spatial step was chosen so that the scaled length of the spatial domain was 2,000 μm long, equivalent to the length of the microfluidic trap used in Kim et al.. Taking into account the design of the trap, Dirichlet (open) boundary conditions were used at the endpoints: $x = 0$ and $x = 2,000\ \mu$m. Additionally, we defined the spatial domain, Ω, to be piecewise by initially breaking it into 100 stripes of equal width (s_1, s_2,..., s_{100}). The activator production terms (η_{a_0}, η_{a_1}) were then defined to be zero for the even numbered stripes while the repressor production terms (η_{r_0}, η_{r_1}) were defined to be zero for the odd numbered stripes. This

created 100, 20 μm wide stripes of alternating activator and repressor producing areas, thereby allowing us to incorporate the columnar spatial patterns observed in Kim et al.. For the P_1N_1 consortia, the production term η_{a_1} was set to 0 everywhere to account for the absence of the positive feedback loop.

Using this scheme, we carried out the synchronization test by first simulating the consortium under study (P_2N_1 or P_1N_1) with initial values of $a_{0,x} = 0$ and $r_{0,x} = 0$ at all spatial points. This resulted in synchronous oscillation of the consortium across the trap. We then extracted the period of this oscillation post-transience, ϕ, and recorded the concentration of a and r for the middle spatial point at time 0.25ϕ. These concentrations were then used to initialize a second simulation. Specifically, in the second simulation, the first 2500 spatial points (the left half of the consortium) were initialized with concentrations $a_{0,x} = 0$ and $r_{0,x} = 0$. The next 2500 spatial points (the right half of the consortium) were initialized with the activator and repressor concentrations extracted from the previous simulation: $a_{0,x} = a_{0.25\phi,2500}$ and $r_{0,x} = r_{0.25\phi,2500}$. This resulted in the left and right halves of the consortium oscillating with the initial phase difference $|\Delta\phi|_0 = 25\%$.

To evaluate whether synchrony occurred, we tracked the activator concentration for the spatial points corresponding to the middle of the left and right sub-populations: $x = 1250$ and $x = 3750$. We then calculated the time difference, Δt_ϕ, between the minima corresponding to the 10th oscillation for these spatial points. This value was then used to calculate the final phase difference using:

$$|\Delta\phi| = \frac{\Delta t_\phi}{\phi} * 100 \tag{33}$$

This process was repeated for both the P_2N_1 and P_1N_1 consortia. In this study, we assumed a phase difference of 2.5% of the period of oscillation, $|\Delta\phi| < 0.025\phi$ corresponded to synchronous oscillation across the trap.

This synchronization test was repeated with slight variations to study the effect of changing the basal production rate and stripe width on the synchronization of the P_1N_1 and P_2N_1 consortia, respectively. To study the effect of changing the basal multiplier on the synchronization of the P_1N_1 consortium, we repeated the P_1N_1 simulations for different values of the basal production rate η_{a_0}. Specifically, we scaled η_{a_0} by a basal multiplier, b_m, and evaluated synchrony for values of b_m ranging from 0.1-10. To evaluate the effect of changing the stripe width on the synchronization of the P_2N_1 consortium, we repeated the P_2N_1 simulations and evaluated synchrony for stripe widths ranging from 200 μm to 10 μm. We took care to choose stripe widths that provided an even number of stripes. This allowed us to properly partition the consortium into two equal halves.

Heterogeneous Stripes Test

To evaluate the effect of heterogeneous stripes on coordination of the P_2N_1 consortium, we again divided the consortium into two halves. However, we modified our numerical scheme so that both halves consisted of stripes whose width increased according to a linear gradient. Specifically, if the half consisted of n_x spatial points and would contain k stripes, we first divided n_x by the sum of the first k numbers. This gave us a common difference, d, which we used to define the number of spatial points in the k-th stripe, n_k: $n_k = kd$. For this study, we used 84 stripes in the left half of the consortium and 14 stripes in the right. These numbers were chosen so that the linear gradient could be properly implemented in each half of the consortium with a manageable number of spatial points equally divided between the halves. This resulted in $n_x = 7,140$ equally spaced spatial points. For this test, we also chose to simulate a larger 4,000 μm consortium which changed our spatial step to $\Delta x = \frac{4000\ \mu\text{m}}{\sqrt{D \cdot \tau}(n_x)}$. All other aspects of our numerical scheme were left unchanged. The numerically implemented system was then simulated with initial values of $a_{0,x} = 0$ and $r_{0,x} = 0$ at all spatial points.

Supporting References

1. Kim J.K., Chen Y., Hirning A.J., Alnahhas R.N., Josić K., Bennett M.R. Long-range temporal coordination of gene expression in synthetic microbial consortia. *Nat Chem Bio* 2019;15(11):1102–9.